

In Vivo Exposure Pathways of Ambient Magnetite Nanoparticles Revealed by Machine Learning-Aided Single-Particle Mass Spectrometry

Weican Zhang, Shiwei Huo, Shenxi Deng, Ke Min, Cha Huang, Hang Yang, Lin Liu, Luyao Zhang, Peijie Zuo, Lihong Liu, Qian Liu,* and Guibin Jiang



Cite This: <https://doi.org/10.1021/acs.nanolett.4c01937>



Read Online

ACCESS |

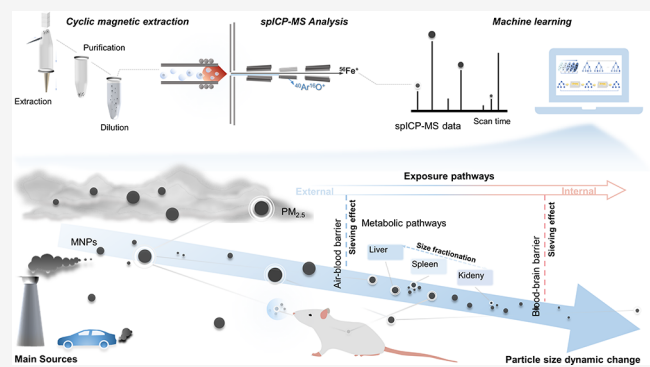
Metrics & More

Article Recommendations

Supporting Information

ABSTRACT: Nanosized ultrafine particles (UFPs) from natural and anthropogenic sources are widespread and pose serious health risks when inhaled by humans. However, tracing the inhaled UFPs *in vivo* is extremely difficult, and the distribution, translocation, and metabolism of UFPs remain unclear. Here, we report a label-free, machine learning-aided single-particle inductively coupled plasma mass spectrometry (spICP-MS) approach for tracing the exposure pathways of airborne magnetite nanoparticles (MNPs), including external emission sources, and distribution and translocation *in vivo* using a mouse model. Our results provide quantitative analysis of different metabolic pathways in mice exposed to MNPs, revealing that the spleen serves as the primary site for MNP metabolism (84.4%), followed by the liver (11.4%). The translocation of inhaled UFPs across different organs alters their particle size. This work provides novel insights into the *in vivo* fate of UFPs as well as a versatile and powerful platform for nanotoxicology and risk assessment.

KEYWORDS: Nanoparticle, Magnetite, Single-particle analysis, Machine learning, Exposure pathway



Atmospheric fine particulate matter (PM_{2.5}, particles with aerodynamic diameter less than 2.5 μm) contributes significantly to global disease burden and mortality in humans.^{1,2} Ultrafine particles (UFPs, particles measuring 100 nm in diameter) represent a serious health hazard compared with coarse particles due to their nanoscale dimensions, which facilitate their circulation in the blood, resulting in adverse health effects.^{3–6} Exogenous magnetite nanoparticles (MNPs), an important toxic species of PM_{2.5}, have been detected in different areas of human body, including brain, blood, heart, pleural effusions, and placental cells, following inhalation.^{4,7–9} These nanoparticles (NPs) in the human body from either anthropogenic or natural sources have been associated with diseases, such as Alzheimer's disease.^{10,11}

Inhalation is the predominant route of exposure to UFPs.¹² The inhaled UFPs deposited in the alveoli may breach the air-blood barrier (ABB) to enter the circulatory system.¹³ The transportation of exogenous particles inside the body is regulated by key biological barriers, such as blood-brain barrier (BBB) and blood-placental barrier. Evidence suggests that UFPs may have potential to penetrate these barriers and invade distal organs or tissues with possible adverse consequences.^{5,7,14} Some organs with large-volume blood circulation, especially liver, spleen, and kidney containing a large number of macrophages or associated with excretion,

tend to be major internal sinks for inhaled UFPs.^{15–17} However, the key mechanisms of internal exposure, such as the states of UFPs in the body, efficiency of penetrating biological barriers, metabolic pathways, and clearance mechanisms are unknown.¹⁸ This seriously hinders the understanding of the systemic health effects of UFPs.

The identification and characterization of UFPs is a prerequisite for assessing their health risks.^{19,20} However, this task is extremely difficult due to the biological matrix and particle dynamics in the body. Currently, chemical or radioactive labeling is primarily used to trace NPs *in vivo*.^{5,21–23} However, the labeling methods interfere with the results due to tag detachment and altered intrinsic properties. Therefore, label-free methods for *in vivo* analysis are of great value. Single-particle inductively coupled plasma mass spectrometry (spICP-MS) provides insight into the elemental composition, concentration, and particle size of NPs at the

Received: April 27, 2024

Revised: June 27, 2024

Accepted: June 27, 2024

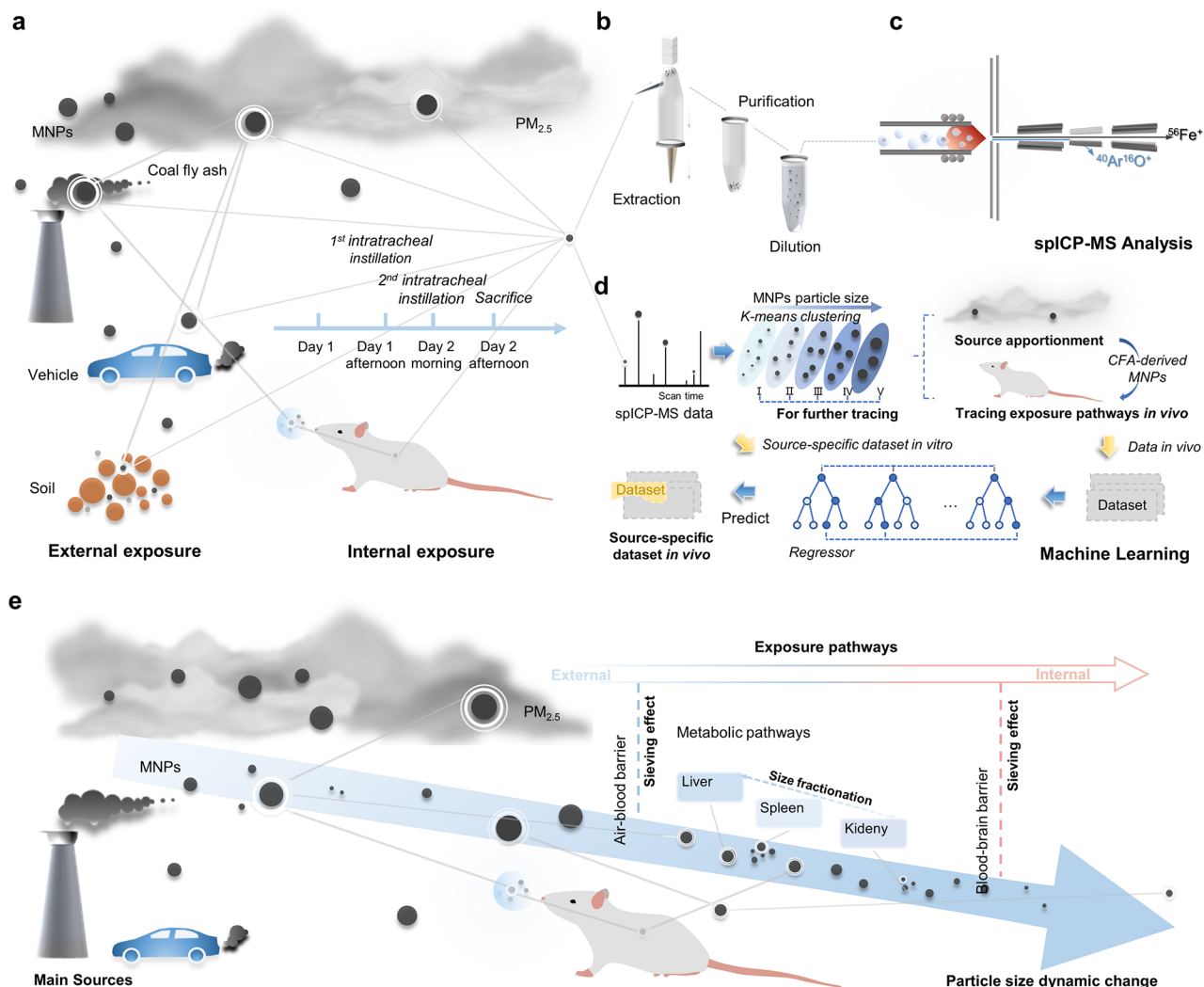


Figure 1. Study design and workflow tracing the exposure pathways of MNPs from the environment to *in vivo*. (a) Typical exogenous sources of MNPs and animal inhalation exposure experiment settings. (b) Procedures for extraction and purification of MNPs from environmental and biological samples. (c) Scheme showing spICP-MS measurements. (d) Workflow of the machine learning-aided spICP-MS analysis. (e) Scheme showing the exposure pathways including external sources and internal translocation and metabolism.

single-particle level rapidly (hundreds of particles per minute) with high sensitivity (detection limit at ng/L level).^{24,25} It reflects the high heterogeneity of particles, and thus provide a more statistically accurate tool than alternative techniques. Because its principle is based on the internal element mass of NPs, it can be used for label-free analysis, especially for NPs containing inert precious metals.²⁶ Multielemental analysis via spICP-MS can also be used to indicate the sources of NPs in the environment.^{27,28} Thus, it is worthwhile to investigate the multidimensional aspects of NPs using spICP-MS linked with the exposure profiles.

To open up the “black box” of internal exposure of inhaled particles,^{4,16} we hypothesized that their physicochemical properties can be changed by the key nodes (e.g., target organs, biological barriers, and circulatory system) in the internal exposure pathways, which may be reflected by spICP-MS analysis and provide pivotal information for tracking the particles’ fate *in vivo*. To test the hypothesis, we established a label-free spICP-MS method and used machine learning to mine MS data to link the particle dynamics to the external sources and internal exposure pathways using MNPs as model UFPs in a mouse model (Figure 1a-d). The results were also

validated via high-resolution morphological fingerprinting using high-angle annular dark-field scanning transmission electron microscopy (HAADF-STEM) and elemental fingerprinting using energy dispersive X-ray energy spectroscopy (EDS). Our results revealed the dynamic particle size variations in the exposure pathways of MNPs (Figure 1e). Notably, we estimated the quantitative contribution of different metabolic pathways of MNPs *in vivo*. By depicting the exposure pathways of MNPs, the critical evidence for supporting the systemic health effects of inhaled UFPs can be obtained.

Due to the extremely low concentration of exogenous MNPs *in vivo* and potential interference by complex biological matrices, appropriate sample preparation is critical for MS analysis.²⁹ We developed a method to efficiently extract MNPs from these matrices while maintaining their original morphology (Supplementary Note 1). Our optimized label-free spICP-MS technique enables multidimensional analysis of MNPs (Supplementary Note 2). Briefly, after effective and selective cyclic magnetic extraction (CME) of MNPs,³⁰ the sample was diluted appropriately to ensure that the individual MNPs are injected into the ICP-MS (Figure 1b). The particle size and

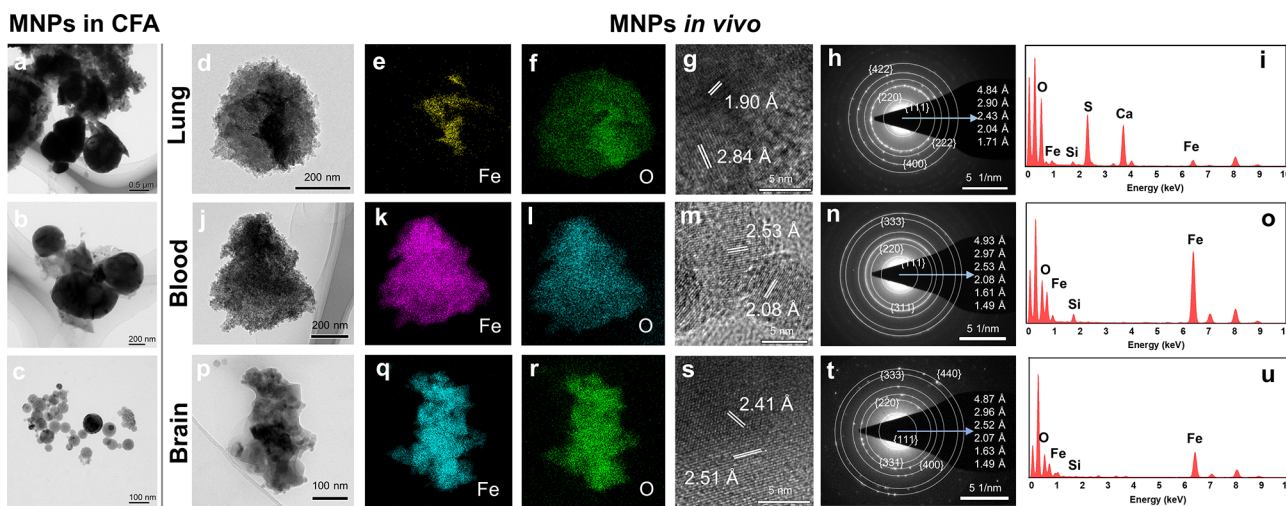


Figure 2. MNPs in environmental and biological samples. (a-c) Coal fly ash. (d-i) Mouse lungs after intratracheal instillation. (j-o) Mouse blood. (p-u) Mouse brain. (a-c,d,j,p) TEM image of MNPs extracted from (a-c) coal fly ash, (d) mouse lungs, (j) mouse blood and (p) mouse brain. (e,f,k,l,q,r) EDS mapping of Fe and O of MNPs extracted from (e,f) mouse lungs, (k,l) mouse blood and (q,r) mouse brain. (g,m,s) Atomic resolution HAADF-STEM images of MNPs extracted from (g) mouse lungs, (m) mouse blood and (s) mouse brain. (h,n,t) Selected area electron diffraction (SAED) patterns of MNPs extracted from (h) mouse lungs, (n) mouse blood and (t) mouse brain. (i,o,u) EDS spectra of MNPs extracted from (i) mouse lung, (o) mouse blood and (u) mouse brain.

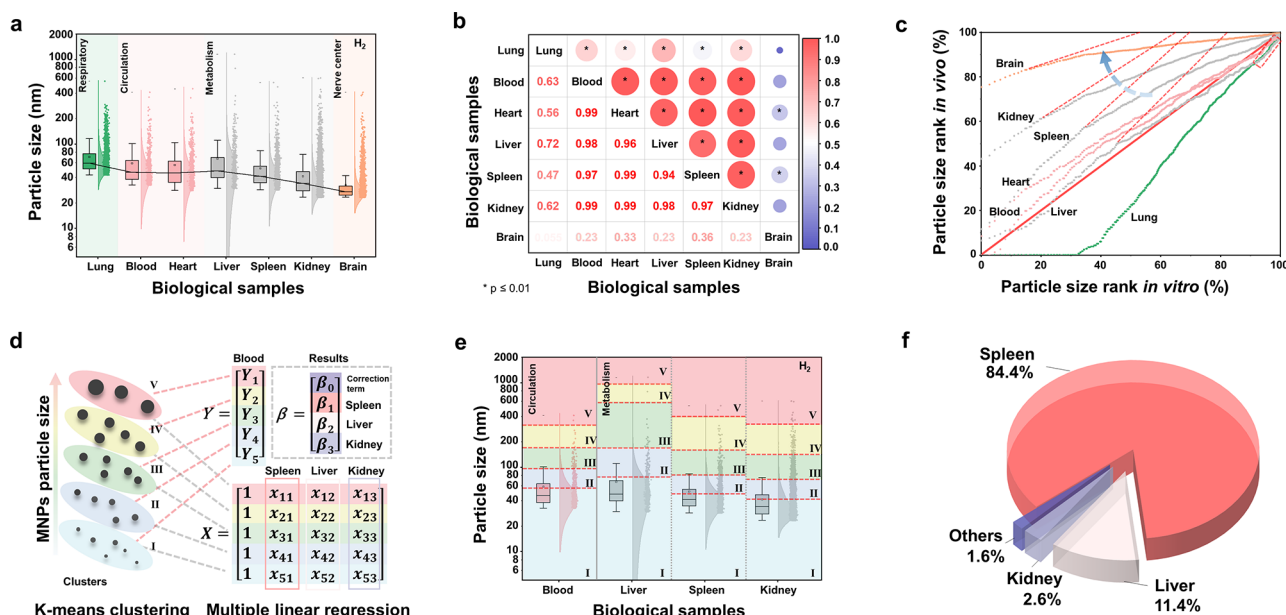


Figure 3. Tracing MNPs *in vivo* via machine learning-aided spICP-MS analysis reveals the dynamics of MNPs in different organs and metabolic pathways. (a) Particle size variation of MNPs in different organs measured by spICP-MS in H₂ mode. The mice were subjected to intratracheal instillation of CFA-derived MNPs ($n = 3$). The boundaries of the box plots span from 25% to 75% percentiles, the center line represents the median, the short black dash represents the maximum, the whisker represents outlier with coefficient 1.5 and the center quadrate represents the mean in (a). The black line in (a) shows the variation trend of particle size in different organs. The colors in (a) indicate the main function of the organs. The results of Dunn's Test in Kruskal-Wallis ANOVA of MNP particle size in biological samples are listed in Table S4. (b) Comprehensive correlation analysis of particle size distribution for MNPs in organs. The particle size distribution of MNPs in each organ was divided into small segments with 5 nm intervals. The overall particle size distribution was described by the particle content between each segment, and correlation analysis was conducted between the particle size distributions in different organs. The size and color of the circles in the upper triangular region of the graph represent the strength of the correlation, with the corresponding color-coded correlation values shown in the legend on the right. The asterisks on the circles indicate statistical significance ($P \leq 0.01$). The lower triangular region of the graph provides the correlation coefficients. (c) The particle size rank variation of MNPs *in vivo* compared with the MNPs *in vitro* (in environment samples) at the single-particle level. The red line shows the unchanged particle size rank from external to internal. The red dash lines show the tangent lines of the rank lines, and the blue dash arrow shows the changing trend of the slope of tangent lines. The red rectangle shows the aggregation of MNPs *in vivo*. (d) The principle of machine learning for tracing the metabolic pathways of MNPs *in vivo*. (e) Cluster analysis results based on spICP-MS analysis of MNPs extracted from the mouse blood, liver, spleen, and kidney in H₂ mode. (f) The contribution of different metabolic pathways to the metabolism of MNPs *in vivo*. The “others” refers to the model error raised by some minor metabolic pathways such as lymph nodes and bone marrow.

number of MNPs was determined simultaneously via spICP-MS equipped with a collision cell by monitoring the $^{56}\text{Fe}^+$ signals (Figure 1c). Additionally, machine learning was employed to extract particle size distribution characteristics of MNPs from different sources for source apportionment of the PM_{2.5}-derived MNPs prior to tracing of MNPs *in vivo* (Figure 1d). The results indicated coal combustion, particularly coal fly ash (CFA), as the primary contributor to airborne MNPs, consistent with previous findings (Figure S1; Supplementary Note 3).³⁰ Note that the sources of airborne MNPs are quite complex, and some other sources such as brake-wear³¹ and iron/steel plant³² with high toxicities also deserve attention.³³

We traced internal exposure routes of MNPs by exposing mice to CFA-derived MNPs via intratracheal instillation at environmental concentrations (Supplementary Note 4). These MNPs, with a wide particle size distribution, reflect the actual state of inhaled MNPs compared with monodisperse MNPs injected intravenously.^{34,35} MNPs detected in mouse blood and organs exhibited larger particle sizes than ferritin,³⁶ with fused interlocking surface crystallites⁴ and characteristic coincident elements (e.g., Si) indicating exogenous origins (Figure 2d-u). In environmental samples, MNPs displayed wide particle size distributions and regular morphology (Figure 2a-c), while *in vivo*, they showed smaller particle sizes and irregular shapes (Figure 2d, j, p). In mouse lungs, MNPs appeared nearly spherical with irregular edges (Figure 2d-f), alongside microsized particles (Figure S2a). In the blood, MNPs occurred as clusters of tiny spheres (Figure 2j-l). Notably, MNPs were also found in the brain (Figure 2p-r) as loose particles and aggregates of smaller subparticles. *In situ* electron microscopic characterization of mouse brain sections further confirmed the accumulation of MNPs in the brain (Figure S3). The particles found by TEM *in vivo* were confirmed as MNPs based on their elemental and structural fingerprints (Figure 2g-i, m-o, s-u). Overall, morphological characterization revealed the alterations in MNP particle size distribution and morphology due to internal exposure processes.

Using spICP-MS, we measured MNP concentration in various mouse organs postexposure, based on number and mass. We found that the ratio of number to mass concentration of MNPs in the lungs and liver is lower than that in the brain, suggesting that more MNPs with larger sizes are present in the lungs and liver than in the brain (Figure S4). Both organs and blood showed exogenous MNP accumulation (Figure S5). Urban PM_{2.5}-derived MNPs also exhibited consistent *in vivo* accumulation, extending the MNP metabolic duration to 7 days from mouse exposure to dissection (Figure S6).

We then investigated the *in vivo* exposure pathways of MNPs based on spICP-MS data. Remarkably, CFA-derived MNPs showed a consistent decrease in particle size across respiratory, circulatory, metabolic organs, and brain, from ~ 60 nm to ~ 30 nm (the median equivalent spherical particle size; Figure 3a). Urban PM_{2.5}-derived MNPs, with a 7-day metabolic duration, exhibited a similar trend, especially for the mouse with the highest lung accumulation of MNPs, except in the brain (Figure S7). The absence of notable alterations in particle size distribution within the brain implied minimal levels of exogenous MNPs, while substantial accumulation occurred in the lungs. Notably, strong correlations were observed in the size distribution of MNPs among blood, heart, liver, spleen,

and kidney, while weaker correlations were seen in the lungs and brain, suggesting the substantial influence of ABB and BBB on MNPs' state *in vivo* (Figure 3b).

To further elucidate the particle size patterns of MNPs *in vivo*, we compared their size rank during external and internal exposure (Figure 3c). We ranked MNPs' sizes from largest (100%) to smallest (0%). When an MNP in the environment was put in the size sorting queue of MNPs in an organ *in vivo*, the size of the particle showed a certain rank variation (i.e., from the abscissa to the ordinate in Figure 3c). Below the red line in Figure 3c, the *in vivo* rank was lower than *in vitro*, indicating possible aggregation *in vivo*, such as in the lungs, liver, blood, and heart. Due to the high chemical stability of magnetite, the half-life of MNPs *in vivo* (ranging from ~ 10 days to more than a year³⁷) was substantially longer than the metabolic time in this study (i.e., ~ 1 day). Thus, the MNPs *in vivo* were not significantly degraded by such exposure. The slope of the particle size in the brain and kidney is significantly different from the other slopes, reflecting the excessive concentration of small particles, which could be attributed to the selective permeability of BBB and the glomerular filtration of NPs.^{38,39} These results indicated that the particle size dynamics depended strongly on the nodes of internal exposure pathways.

MNPs in the metabolic organs were transported via the blood circulation, as evidenced by high relevancy of size distribution of MNPs in the circulatory system with the liver, spleen, and kidney (Figure 3b). Machine learning was employed to extract the particle size distribution characteristics of MNPs in various metabolic organs. Considering the compact and distinct clusters obtained by machine learning,⁴⁰ the influence of metabolic process could be reflected by the size range variations of the clusters in the blood and different organs (Figure 3d, e; Figure S8 for detailed cluster ranges). Due to the high stability of MNPs and the short metabolic duration, intercluster conversion of particles (i.e., a particle shifted from one cluster to another cluster) across the different nodes of internal exposure from blood to the metabolic organs was negligible. Nonetheless, the potential loss of particle number of MNPs targeting the different metabolic organs due to aggregation, complete degradation/dissolution, etc., was represented by a correction factor (*E*) (Figure S9; Supplementary Note 5). Thus, a robust model was established for *in vivo* analysis (see eq (1) in Materials and Methods Supporting Information). Using a multiple linear regression model to evaluate the different parameters (Figure 3d), based on eq (1) Supporting Information, we estimated the quantitative contributions of different metabolic pathways of MNPs *in vivo*, especially involving spleen ($84.4 \pm 4.2\%$), followed by liver ($11.4 \pm 0.7\%$) and kidney ($2.6 \pm 4.1\%$) (Figure 3f). The contribution of other possible metabolic pathways (e.g., lymph nodes and bone marrow) and tissues throughout the body to accumulate MNPs was also considered (see eq (2) in Materials and Methods Supporting Information) and estimated at about 1.6%. The excellent fitness and the uncertainty based on the error propagation calculation of the model demonstrated the feasibility of the results (Table S1).

In this model, the cluster center (i.e., the average of the data in a cluster) indicated that MNPs with different particle sizes tended to target different metabolic organs (Supplementary Note 6). The liver retained most of the Cluster 1 and 5 particles, while the spleen accumulated most of the medium-sized particles (Figure S10). The kidney was significantly

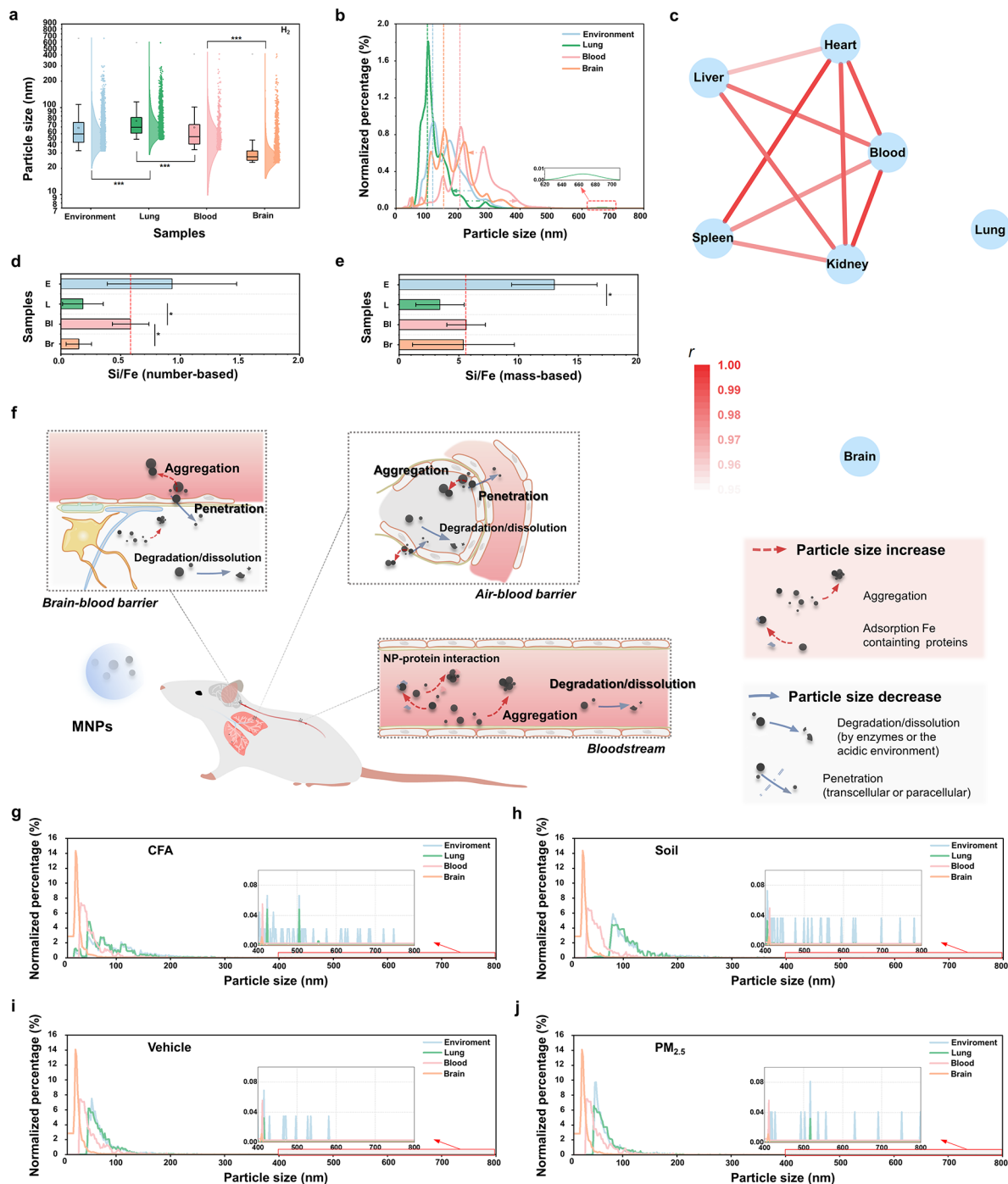


Figure 4. Insights into the mechanisms of dynamic particle size variations of MNPs *in vivo*. Particle size variations of MNPs from environmental media (CFA) to biological samples (extracted from mouse organs after intratracheal instillation of CFA-derived MNPs) measured by (a) spICP-MS in H₂ mode and (b) nanoparticle tracking analysis (NTA). The “***” in (a) refers to $P < 0.001$, Mann–Whitney U test. The boundaries of the box plots span from 25% to 75% percentile, the center line represents the median, the short black dash represents the maximum, the whisker represents outlier with coefficient 1.5, and the center quadrate represents the mean in (a). The dashed lines in (b) show the maximum peak value of the distribution curve. Arrows in (b) highlight the particle size change when MNPs crossing the biological barriers. The red dotted rectangle in (b) indicates the aggregation of MNPs in the lungs. (c) The network analysis based on comprehensive correlation analysis of particle size fingerprints of MNPs in the biological samples. The particle size distribution is divided into several bins with the size of 10 nm for the correlation analysis. The lines in the network are colored based on the r (correlation coefficient) values. The lines with $r < 0.95$ are not shown in the figure. (d,e) The Si/Fe elemental fingerprinting of MNPs in the environmental (E) and biological samples (i.e., the lungs (L), blood (Bl) and brain (Br)) measured by spICP-MS and calculated by $(\text{SiO}_2 \text{ NPs}) / (\text{Fe}_3\text{O}_4 \text{ NPs})$ by particle number (d) and particle mass (e). The error bars represent 1 s.d. for the results ($n = 3$). The “*” means $P < 0.05$. $P_{\text{Lung-Blood}} = 0.039$, $P_{\text{Blood-Brain}} = 0.016$, unpaired Student's two-tailed t -test in (d). $P_{\text{Environment-Lung}} = 0.016$, unpaired Student's two-tailed t -test in (e). (f) Scheme showing the possible mechanisms for dynamics of MNPs when crossing the biological barriers (i.e., air-blood and brain-blood barriers) and being translocated in the bloodstream. The main possible processes causing the particle size change *in vivo* are in bold. (g-j) The prediction results of *in vivo* particle size distribution in different organs of MNPs derived from different sources ((g) CFA, (h) soil, (i) vehicle and (j) PM_{2.5}). The subgraph in each figure shows the results for large particles (400–800 nm).

enriched in small particles reflected by the contribution of Cluster 1. Overall, large (ca. 500–1,000 nm) and small (ca. 15–40 nm) particles in the blood tended to accumulate in the liver, whereas medium-sized particles (ca. 40–300 nm) were diverted to the spleen, and tiny particles (ca. 0–15 nm) were transported to the kidney. This result can be explained by multiple particle size-dependent mechanisms, such as particle recognition (e.g., Kupffer cells in the liver), entrapment (e.g., Disse space in the liver), and filtration (e.g., splenic filtration and kidney fenestrae) in these metabolic organs.^{15,35} The real-world MNPs used in the experiments contained a high percentage of medium-sized particles (Figure S1b), explaining the spleen's role as the primary organ for metabolism. MNPs entering the spleen are primarily filtered by macrophages located in the red pulp and marginal zones, followed by filtration in the macrophages lining the venous sinuses.⁴¹ A few NPs may also enter the white pulp composed mainly of lymphatic tissue, triggering an immune response.⁴²

Due to the high background of Fe in biological matrix and interference from nonparticulate Fe-containing species, the total MNP content was difficult to quantify by normal ICP-MS method based on the elemental signal of Fe. Magnetic methods struggle to quantify real-world MNPs in mice due to great heterogeneity. Our method overcomes these obstacles, providing quantitative insights into metabolic pathways. Although most of the previous studies show higher NP absorption in the liver than the spleen, the precise contribution of liver and spleen in the translocation of NPs was still ambiguous (Table S2). Our results underscore the necessity to investigate the spleen's role in the metabolism of UFPs for evaluating the risk of MNP accumulation *in vivo*.

The particle size of MNPs increased after entering the mice lungs, but varied widely in the blood and a decline trend in the brain (Figure 4a). The findings were validated via nanoparticle tracking analysis (NTA) (Figure 4b) and morphological characterization (Figure 2d, j, p; Figure S2). Parallel to the correlation analysis (Figure 3b), the network analysis demonstrated a substantial “sieving” effect across organs, a phenomenon intricately associated with and influenced by the interaction of biological macromolecules, segregating the lungs and brain from other organs in the exposure pathways of MNPs (Figure 4c).

To elucidate the mechanism of size fractionation of MNPs *in vivo*, we also used Si/Fe chemical fingerprints obtained from spICP-MS (Figure 4d, e). Si is commonly found in MNPs (Figure S11e, o, w) and is less reactive than Fe *in vivo*.^{43,44} Thus, Si can be used as an auxiliary elemental marker of MNPs to evaluate the particle exposure behavior. Our findings indicated that the ratio of Si/Fe decreased from the environment to the lungs, suggesting that large particles containing higher levels of Si were more difficult to enter into the lungs.⁴⁵ Following translocation of MNPs into the blood, the Si/Fe ratio was increased, probably due to the degradation or transformation of Fe species in the blood (e.g., through dissolution in the endosomes or lysosomes within an acidic environment and enzymes present in macrophages^{46,47}). Further, the Si/Fe ratio based on the particle number increased more significantly than the ratio based on mass concentration, which may be attributed to the aggregation of small particles in the blood, based on TEM (Figure 2j) and SEM results (Figure S2f, k). The aggregation may promote the conversion of small particles with high Fe content to fewer large particles of Fe-containing NPs. Such aggregation may take place during the

adsorption of plasma proteins (e.g., fibrinogen), influenced by weak steric hindrance or electrostatic repulsion forces.^{35,48} Penetration of the BBB was a major factor altering the particle size of MNPs across the blood and brain. The Si/Fe mass ratio during the penetration of the BBB did not change significantly, suggesting that MNPs in the brain did not degrade obviously. However, the Si/Fe ratio based on number decreased significantly, indicating the prevention of large MNPs entering the brain by the BBB.

Based on the foregoing results, we summarize the main mechanisms affecting the particle size distribution of MNPs penetrating biological barriers *in vivo* (Figure 4f). Particle aggregation³⁵ and interactions with plasma proteins^{48,49} contribute to an increase in particle size, while enzymatic or acidic degradation/dissolution^{35,50} and penetration through transcellular (e.g., transcytosis, receptor-mediated transportation, and diffusion) and paracellular (i.e., across intercellular junctions)^{51,52} routes can lead to a reduction in particle size. Due to the cellular internalization of NPs⁵¹ and the pore size-limited translocation (e.g., drain via the stomata in the parietal pleura^{53,54}), the biological barriers may be impenetrable for large NPs, resulting in decreased particle size after penetration.

Considering the source-specific nature of MNPs' particle size patterns (Figure S1a-c), we predicted and compared the *in vivo* size distribution of MNPs from different sources at various exposure nodes (Figure S12). Accordingly, a reliable model employing gradient boosting and random forest algorithms was constructed (Table S3). The model could “learn” how the particle size distribution of MNPs affects the internal MNP exposure based on the particle size of CFA-derived MNPs and their corresponding sizes in various organs. Subsequently, it could predict the particle size distribution of MNPs from other sources *in vivo* to show their passage through biological barriers and fate. It should be noted that only particle size distribution information was used as input in the model training, which makes the model applicable for diverse sources rather than a specific source. Therefore, the morphological characteristics and elemental compositions of MNPs would not affect the predictive results because these kinds of information were not used in the model training. Including more information on MNPs in the model may further enhance the model performance in the future.

Particle distribution curves of MNPs in the blood and brain exhibited similarities across diverse sources, while lung distributions closely resembled those of external sources (Figure 4g-j). The size distribution of MNPs in the blood and brain displayed reduced source specificity, particularly in the brain. This implied that the presence of biological barriers might weaken the linkage between exogenous particles located deep within the body and their respective sources. For the two main sources of MNPs, CFA and traffic (Figure S1i), traffic sources released finer MNPs capable of penetrating the BBB and reaching the brain. In contrast, combustion sources generated particles that predominantly accumulated in the lungs, leading to adverse respiratory effects. This finding was also in line with epidemiological studies concerning PM_{2.5} in typical areas,^{11,55} which offers novel and reliable explanations for the link between MNP sources and diseases. Understanding MNP exposure pathways enhances toxicity correlation with external sources, thereby aiding targeted health risk mitigation strategies. At the same time, we agree that including more information on MNPs in the model will further enhance the

model performance, which will be considered in our future studies.

In summary, this study provides a versatile platform for particulate toxicology and NP risk assessment to trace the exposure pathway of inhaled MNPs using machine learning-aided spICP-MS. This label-free, high-throughput, and information-rich platform can reveal the external exposure sources and internal exposure fate of MNPs. Our results reveal the quantitative role of different organs, primarily spleen (84.4%), followed by liver (11.4%) and kidney (2.6%), in the metabolism of MNPs. It should also be noted that this work is a “snap-shot” of NPs *in vivo*. Further longitudinal studies with longer exposure duration and different PM_{2.5} species are required, and the results also need to be verified in cells or even human body. Only with comprehensive analytical methodology combining with advanced models, we can elaborate the *in vivo* fate of UFPs and link together the external pollutant exposure, internal exposure dose, biological response, and health outcome to form full-chain evidence for the health effect of particulate exposure.

■ ASSOCIATED CONTENT

SI Supporting Information

The Supporting Information is available free of charge at <https://pubs.acs.org/doi/10.1021/acs.nanolett.4c01937>.

Notes providing supplementary discussion on development and optimization of the sample preparation method for MNPs in biological samples, the optimization of spICP-MS analysis method for MNPs, characterization of MNPs from typical sources and source apportionment of MNPs, estimation of exposure dose of MNPs for mice, possible particle number variation when MNPs target to metabolic organs, and understandings of the translocation and metabolism pathways of MNPs from the cluster center; figures presenting the additional data on machine learning-aided spICP-MS analysis for external source apportionment of MNPs, morphological, structural, elemental fingerprinting and particle size distribution of MNPs in environmental samples and mice organs, the optimization and evaluation of machine learning-aided spICP-MS analysis method, and some possible mechanisms responsible for particle number variations of MNPs during the translocation and metabolic pathways *in vivo*; tables presenting information about results of multiple linear regression modeling, summary of some studies about the metabolism of NPs in the liver and spleen, valuation parameters of prediction models, results of Dunn's Test in Kruskal-Wallis ANOVA of MNP particle size in biological samples, parameters of ICP-MS for single-particle analysis, and quantification results of MNPs in different environmental samples ([PDF](#))

■ AUTHOR INFORMATION

Corresponding Author

Qian Liu – State Key Laboratory of Environmental Chemistry and Ecotoxicology, Research Center for Eco-Environmental Sciences, Chinese Academy of Sciences, Beijing 100085, China; University of Chinese Academy of Sciences, Beijing 100190, China; Institute of Environment and Health, Jianghan University, Wuhan 430056, China; [orcid.org/0000-0001-8525-7961](#); Email: qianliu@rcees.ac.cn

Authors

Weican Zhang – State Key Laboratory of Environmental Chemistry and Ecotoxicology, Research Center for Eco-Environmental Sciences, Chinese Academy of Sciences, Beijing 100085, China; University of Chinese Academy of Sciences, Beijing 100190, China; [orcid.org/0000-0002-8730-2778](#)

Shiwei Huo – State Key Laboratory of Environmental Chemistry and Ecotoxicology, Research Center for Eco-Environmental Sciences, Chinese Academy of Sciences, Beijing 100085, China; University of Chinese Academy of Sciences, Beijing 100190, China

Shenxi Deng – State Key Laboratory of Environmental Chemistry and Ecotoxicology, Research Center for Eco-Environmental Sciences, Chinese Academy of Sciences, Beijing 100085, China; School of Public Health, Li Ka Shing Faculty of Medicine, The University of Hong Kong, Hong Kong SAR, China

Ke Min – State Key Laboratory of Environmental Chemistry and Ecotoxicology, Research Center for Eco-Environmental Sciences, Chinese Academy of Sciences, Beijing 100085, China; [orcid.org/0000-0003-4345-7855](#)

Cha Huang – State Key Laboratory of Environmental Chemistry and Ecotoxicology, Research Center for Eco-Environmental Sciences, Chinese Academy of Sciences, Beijing 100085, China; University of Chinese Academy of Sciences, Beijing 100190, China

Hang Yang – State Key Laboratory of Environmental Chemistry and Ecotoxicology, Research Center for Eco-Environmental Sciences, Chinese Academy of Sciences, Beijing 100085, China; University of Chinese Academy of Sciences, Beijing 100190, China

Lin Liu – State Key Laboratory of Environmental Chemistry and Ecotoxicology, Research Center for Eco-Environmental Sciences, Chinese Academy of Sciences, Beijing 100085, China; University of Chinese Academy of Sciences, Beijing 100190, China

Luyao Zhang – State Key Laboratory of Environmental Chemistry and Ecotoxicology, Research Center for Eco-Environmental Sciences, Chinese Academy of Sciences, Beijing 100085, China; University of Chinese Academy of Sciences, Beijing 100190, China

Peijie Zuo – State Key Laboratory of Environmental Chemistry and Ecotoxicology, Research Center for Eco-Environmental Sciences, Chinese Academy of Sciences, Beijing 100085, China; University of Chinese Academy of Sciences, Beijing 100190, China

Lihong Liu – State Key Laboratory of Environmental Chemistry and Ecotoxicology, Research Center for Eco-Environmental Sciences, Chinese Academy of Sciences, Beijing 100085, China

Guibin Jiang – State Key Laboratory of Environmental Chemistry and Ecotoxicology, Research Center for Eco-Environmental Sciences, Chinese Academy of Sciences, Beijing 100085, China; University of Chinese Academy of Sciences, Beijing 100190, China; [orcid.org/0000-0002-6335-3917](#)

Complete contact information is available at:
<https://pubs.acs.org/doi/10.1021/acs.nanolett.4c01937>

Author Contributions

Q.L. and W.Z. conceived and designed the research; W.Z. performed most of experiments; S.H. and S.D. helped with the animal experiments; H.Y., Lin L., and P.Z. collected the samples and helped with the particle extraction; C.H. and

Lihong L. helped with spICP-MS data processing; K.M., S.D., H.Y., C.H. and L.Z. commented on the manuscript; G.J. supervised the project; W.Z. and Q.L. analyzed the data; W.Z. and Q.L. wrote the paper.

Notes

The authors declare no competing financial interest.

ACKNOWLEDGMENTS

This work was financially supported by National Key R&D Program of China (2023YFC3708302), National Natural Science Foundation of China (Nos. 22425041, 22188102, 22193050), and Chinese Academy of Sciences Project for Young Scientists in Basic Research (YSBR-086). Q.L. acknowledges the support from the XPLORER Prize.

REFERENCES

- (1) Schmale, J.; Shindell, D.; von Schneidemesser, E.; Chabay, I.; Lawrence, M. Air Pollution: Clean up Our Skies. *Nature* **2014**, *515*, 335–337.
- (2) Cohen, A. J.; Brauer, M.; Burnett, R.; Anderson, H. R.; Frostad, J.; Estep, K.; Balakrishnan, K.; Brunekreef, B.; Dandona, L.; Dandona, R.; Feigin, V.; Freedman, G.; Hubbell, B.; Jobling, A.; Kan, H.; Knibbs, L.; Liu, Y.; Martin, R.; Morawska, L.; Pope, C. A.; Shin, H.; Straif, K.; Shaddick, G.; Thomas, M.; van Dingenen, R.; van Donkelaar, A.; Vos, T.; Murray, C. J. L.; Forouzanfar, M. H. Estimates and 25-Year Trends of the Global Burden of Disease Attributable to Ambient Air Pollution: An Analysis of Data from the Global Burden of Diseases Study 2015. *Lancet* **2017**, *389*, 1907–1918.
- (3) Oberdorster, G.; Oberdorster, E.; Oberdorster, J. Nanotoxicology: An Emerging Discipline Evolving from Studies of Ultrafine Particles. *Environ. Health Perspect.* **2005**, *113*, 823–839.
- (4) Lu, D.; Luo, Q.; Chen, R.; Zhusansun, Y.; Jiang, J.; Wang, W.; Yang, X.; Zhang, L.; Liu, X.; Li, F.; Liu, Q.; Jiang, G. Chemical Multi-Fingerprinting of Exogenous Ultrafine Particles in Human Serum and Pleural Effusion. *Nat. Commun.* **2020**, *11*, 2567.
- (5) Qi, Y.; Wei, S.; Xin, T.; Huang, C.; Pu, Y.; Ma, J.; Zhang, C.; Liu, Y.; Lynch, I.; Liu, S. Passage of Exogeneous Fine Particles from the Lung into the Brain in Humans and Animals. *Proc. Natl. Acad. Sci. U. S. A.* **2022**, *119*, No. e2117083119.
- (6) Miller, M. R.; Raftis, J. B.; Langrish, J. P.; McLean, S. G.; Samutrtai, P.; Connell, S. P.; Wilson, S.; Vesey, A. T.; Fokkens, P. H. B.; Boere, A. J. F.; Krystek, P.; Campbell, C. J.; Hadoke, P. W. F.; Donaldson, K.; Cassee, F. R.; Newby, D. E.; Duffin, R.; Mills, N. L. Inhaled Nanoparticles Accumulate at Sites of Vascular Disease. *ACS Nano* **2017**, *11*, 4542–4552.
- (7) Maher, B. A.; Ahmed, I. A. M.; Karloukovski, V.; McLaren, D. A.; Foulds, P. G.; Allsop, D.; Mann, D. M. A.; Torres-Jardon, R.; Calderon-Garcidueñas, L. Magnetite Pollution Nanoparticles in the Human Brain. *Proc. Natl. Acad. Sci. U. S. A.* **2016**, *113*, 10797–10801.
- (8) Calderón-Garcidueñas, L.; González-Maciel, A.; Mukherjee, P. S.; Reynoso-Robles, R.; Pérez-Guillé, B.; Gayosso-Chávez, C.; Torres-Jardón, R.; Cross, J. V.; Ahmed, I. A. M.; Karloukovski, V. V.; Maher, B. A. Combustion- and Friction-Derived Magnetic Air Pollution Nanoparticles in Human Hearts. *Environ. Res.* **2019**, *176*, No. 108567.
- (9) Liu, N. M.; Miyashita, L.; Maher, B. A.; McPhail, G.; Jones, C. J. P.; Barratt, B.; Thangaratinam, S.; Karloukovski, V.; Ahmed, I. A.; Aslam, Z.; Grigg, J. Evidence for the Presence of Air Pollution Nanoparticles in Placental Tissue Cells. *Sci. Total Environ.* **2021**, *751*, No. 142235.
- (10) Maher, B. A. Airborne Magnetite- and Iron-Rich Pollution Nanoparticles: Potential Neurotoxicants and Environmental Risk Factors for Neurodegenerative Disease, Including Alzheimer's Disease. *J. Alzheimers Dis.* **2019**, *71*, 361–375.
- (11) Calderón-Garcidueñas, L.; Villarreal-Ríos, R. Living Close to Heavy Traffic Roads, Air Pollution, and Dementia. *Lancet* **2017**, *389*, 675–677.
- (12) De Matteis, V. Exposure to Inorganic Nanoparticles: Routes of Entry, Immune Response, Biodistribution and *In Vitro/In Vivo* Toxicity Evaluation. *Toxics* **2017**, *5*, 29.
- (13) Shimada, A.; Kawamura, N.; Okajima, M.; Kaewamatawong, T.; Inoue, H.; Morita, T. Translocation Pathway of the Intratracheally Instilled Ultrafine Particles from the Lung into the Blood Circulation in the Mouse. *Toxicol. Pathol.* **2006**, *34*, 949–957.
- (14) Bove, H.; Bongaerts, E.; Slenders, E.; Bijnens, E. M.; Saenen, N. D.; Gyselaers, W.; Van Eyken, P.; Plusquin, M.; Roeflaers, M. B. J.; Ameloot, M.; Nawrot, T. S. Ambient Black Carbon Particles Reach the Fetal Side of Human Placenta. *Nat. Commun.* **2019**, *10*, 3866.
- (15) Weissleder, R.; Nahrendorf, M.; Pittet, M. J. Imaging Macrophages with Nanoparticles. *Nat. Mater.* **2014**, *13*, 125–138.
- (16) Cao, M.; Cai, R.; Zhao, L.; Guo, M.; Wang, L.; Wang, Y.; Zhang, L.; Wang, X.; Yao, H.; Xie, C.; Cong, Y.; Guan, Y.; Tao, X.; Wang, Y.; Xu, S.; Liu, Y.; Zhao, Y.; Chen, C. Molybdenum Derived from Nanomaterials Incorporates into Molybdenum Enzymes and Affects Their Activities *In Vivo*. *Nat. Nanotechnol.* **2021**, *16*, 708–716.
- (17) Bakand, S.; Hayes, A. Toxicological Considerations, Toxicity Assessment, and Risk Management of Inhaled Nanoparticles. *Int. J. Mol. Sci.* **2016**, *17*, 929.
- (18) Wang, W.; Lin, Y.; Yang, H.; Ling, W.; Liu, L.; Zhang, W.; Lu, D.; Liu, Q.; Jiang, G. Internal Exposure and Distribution of Airborne Fine Particles in the Human Body: Methodology, Current Understandings, and Research Needs. *Environ. Sci. Technol.* **2022**, *56*, 6857–6869.
- (19) Malysheva, A.; Lombi, E.; Voelcker, N. H. Bridging the Divide between Human and Environmental Nanotoxicology. *Nat. Nanotechnol.* **2015**, *10*, 835–844.
- (20) Jiang, C.; Liu, S.; Zhang, T.; Liu, Q.; Alvarez, P. J. J.; Chen, W. Current Methods and Prospects for Analysis and Characterization of Nanomaterials in the Environment. *Environ. Sci. Technol.* **2022**, *56*, 7426–7447.
- (21) Li, D.; Li, Y.; Li, G.; Zhang, Y.; Li, J.; Chen, H. Fluorescent Reconstitution on Deposition of PM_{2.5} in Lung and Extrapulmonary Organs. *Proc. Natl. Acad. Sci. U. S. A.* **2019**, *116*, 2488–2493.
- (22) Luo, Y.; Li, L.; Feng, Y.; Li, R.; Yang, J.; Peijnenburg, W. J. G. M.; Tu, C. Quantitative Tracing of Uptake and Transport of Submicrometre Plastics in Crop Plants Using Lanthanide Chelates as a Dual-Functional Tracer. *Nat. Nanotechnol.* **2022**, *17*, 424–431.
- (23) Chen, H.; Hu, Q.; Li, W.; Cai, X.; Mao, L.; Li, R. Approaches to Nanoparticle Labeling: A Review of Fluorescent, Radiological, and Metallic Techniques. *Environ. Health* **2023**, *1*, 75–89.
- (24) Huang, X.; Liu, H.; Lu, D.; Lin, Y.; Liu, J.; Liu, Q.; Nie, Z.; Jiang, G. Mass Spectrometry for Multi-Dimensional Characterization of Natural and Synthetic Materials at the Nanoscale. *Chem. Soc. Rev.* **2021**, *50*, 5243–5280.
- (25) Laborda, F.; Bolea, E.; Jiménez-Lamana, J. Single Particle Inductively Coupled Plasma Mass Spectrometry: A Powerful Tool for Nanoanalysis. *Anal. Chem.* **2014**, *86*, 2270–2278.
- (26) Sun, Y.; Liu, N.; Wang, Y.; Yin, Y.; Qu, G.; Shi, J.; Song, M.; Hu, L.; He, B.; Liu, G.; Cai, Y.; Liang, Y.; Jiang, G. Monitoring AuNP Dynamics in the Blood of a Single Mouse Using Single Particle Inductively Coupled Plasma Mass Spectrometry with an Ultralow-Volume High-Efficiency Introduction System. *Anal. Chem.* **2020**, *92*, 14872–14877.
- (27) Praetorius, A.; Gundlach-Graham, A.; Goldberg, E.; Fabienke, W.; Navratilova, J.; Gondikas, A.; Kaegi, R.; Günther, D.; Hofmann, T.; von der Kammer, F. Single-Particle Multi-Element Fingerprinting (spMEF) Using Inductively-Coupled Plasma Time-of-Flight Mass Spectrometry (ICP-TOFMS) to Identify Engineered Nanoparticles against the Elevated Natural Background in Soils. *Environ. Sci.: Nano* **2017**, *4*, 307–314.
- (28) Bland, G. D.; Battifarano, M.; Pradas del Real, A. E.; Sarret, G.; Lowry, G. V. Distinguishing Engineered TiO₂ Nanomaterials from Natural Ti Nanomaterials in Soil Using spICP-TOFMS and Machine Learning. *Environ. Sci. Technol.* **2022**, *56*, 2990–3001.
- (29) Abdolahpur Monikh, F.; Guo, Z.; Zhang, P.; Vijver, M. G.; Lynch, I.; Valsami-Jones, E.; Peijnenburg, W. J. G. M. An Analytical

- Workflow for Dynamic Characterization and Quantification of Metal-Bearing Nanomaterials in Biological Matrices. *Nat. Protoc.* **2022**, *17*, 1926–1952.
- (30) Zhang, Q.; Lu, D.; Wang, D.; Yang, X.; Zuo, P.; Yang, H.; Fu, Q.; Liu, Q.; Jiang, G. Separation and Tracing of Anthropogenic Magnetite Nanoparticles in the Urban Atmosphere. *Environ. Sci. Technol.* **2020**, *54*, 9274–9284.
- (31) Gonet, T.; Maher, B. A.; Nyirő-Kósa, I.; Pósfai, M.; Vaculík, M.; Kukutschová, J. Size-resolved, quantitative evaluation of the magnetic mineralogy of airborne brake-wear particulate emissions. *Environ. Pollut.* **2021**, *288*, No. 117808.
- (32) Li, S.; Zhang, B.; Wu, D.; Li, Z.; Chu, S.-Q.; Ding, X.; Tang, X.; Chen, J.; Li, Q. Magnetic Particles Unintentionally Emitted from Anthropogenic Sources: Iron and Steel Plants. *Environ. Sci. Technol. Lett.* **2021**, *8*, 295–300.
- (33) Cui, W.; Ma, Z.; Chen, Y.; Li, S.; Wu, D.; Chen, X.; Shao, Y.; Liu, Y.; Li, Q.; Chen, J. High Magnetic Property and Toxicity of Particulate Matter Generated during Welding and Cutting Processes. *Environ. Health* **2024**, *2*, 381–389.
- (34) Xu, M.; Niu, Z.; Liu, C.; Yan, J.; Peng, B.; Yang, Y. Oxidative Potential of Metal-Containing Nanoparticles in Coal Fly Ash Generated from Coal-Fired Power Plants in China. *Environ. Health* **2023**, *1*, 180–190.
- (35) Arami, H.; Khandhar, A.; Liggitt, D.; Krishnan, K. M. *In Vivo* Delivery, Pharmacokinetics, Biodistribution and Toxicity of Iron Oxide Nanoparticles. *Chem. Soc. Rev.* **2015**, *44*, 8576–8607.
- (36) Kirschvink, J. L.; Kobayashi-Kirschvink, A.; Woodford, B. J. Magnetite Biomineralization in the Human Brain. *Proc. Natl. Acad. Sci. U. S. A.* **1992**, *89*, 7683–7687.
- (37) Zelepukin, I. V.; Yaremenko, A. V.; Ivanov, I. N.; Yuryev, M. V.; Cherkasov, V. R.; Deyev, S. M.; Nikitin, P. I.; Nikitin, M. P. Long-Term Fate of Magnetic Particles in Mice: A Comprehensive Study. *ACS Nano* **2021**, *15*, 11341–11357.
- (38) Zhou, Y.; Peng, Z.; Seven, E. S.; Leblanc, R. M. Crossing the Blood-Brain Barrier with Nanoparticles. *J. Controlled Release* **2018**, *270*, 290–303.
- (39) Du, B.; Yu, M.; Zheng, J. Transport and Interactions of Nanoparticles in the Kidneys. *Nat. Rev. Mater.* **2018**, *3*, 358–374.
- (40) Huang, X.; Ye, Y.; Zhang, H. Extensions of Kmeans-Type Algorithms: A New Clustering Framework by Integrating Intracluster Compactness and Intercluster Separation. *IEEE Trans. Neural Netw. Learn. Syst.* **2014**, *25*, 1433–1446.
- (41) Feliu, N.; Docter, D.; Heine, M.; del Pino, P.; Ashraf, S.; Kolosnjaj-Tabi, J.; Macchiarini, P.; Nielsen, P.; Alloyeau, D.; Gazeau, F.; Stauber, R. H.; Parak, W. J. *In Vivo* Degeneration and the Fate of Inorganic Nanoparticles. *Chem. Soc. Rev.* **2016**, *45*, 2440–2457.
- (42) Elci, S. G.; Jiang, Y.; Yan, B.; Kim, S. T.; Saha, K.; Moyano, D. F.; Yesilbag Tonga, G.; Jackson, L. C.; Rotello, V. M.; Vachet, R. W. Surface Charge Controls the Suborgan Biodistributions of Gold Nanoparticles. *ACS Nano* **2016**, *10*, 5536–5542.
- (43) Ehrlich, H.; Demadis, K. D.; Pokrovsky, O. S.; Koutsoukos, P. G. Modern Views on Desilicification: Biosilica and Abiotic Silica Dissolution in Natural and Artificial Environments. *Chem. Rev.* **2010**, *110*, 4656–4689.
- (44) Li, J.; Yuan, Z.; Liu, H.; Feng, J.; Chen, Z. Size-Dependent Tissue-Specific Biological Effects of Core–Shell Structured $\text{Fe}_3\text{O}_4@\text{SiO}_2-\text{NH}_2$ Nanoparticles. *J. Nanobiotechnol.* **2019**, *17*, 124.
- (45) Lanzerstorfer, C. Fly Ash from Coal Combustion: Dependence of the Concentration of Various Elements on the Particle Size. *Fuel* **2018**, *228*, 263–271.
- (46) Zhu, M.; Wang, B.; Wang, Y.; Yuan, L.; Wang, H.; Wang, M.; Ouyang, H.; Chai, Z.; Feng, W.; Zhao, Y. Endothelial Dysfunction and Inflammation Induced by Iron Oxide Nanoparticle Exposure: Risk Factors for Early Atherosclerosis. *Toxicol. Lett.* **2011**, *203*, 162–171.
- (47) MacParland, S. A.; Tsoi, K. M.; Ouyang, B.; Ma, X.-Z.; Manuel, J.; Fawaz, A.; Ostrowski, M. A.; Alman, B. A.; Zilman, A.; Chan, W. C.; W.; McGilvray, I. D. Phenotype Determines Nanoparticle Uptake by Human Macrophages from Liver and Blood. *ACS Nano* **2017**, *11*, 2428–2443.
- (48) Kolosnjaj-Tabi, J.; Lartigue, L.; Javed, Y.; Luciani, N.; Pellegrino, T.; Wilhelm, C.; Alloyeau, D.; Gazeau, F. Biotransformations of Magnetic Nanoparticles in the Body. *Nano Today* **2016**, *11*, 280–284.
- (49) Lartigue, L.; Wilhelm, C.; Servais, J.; Factor, C.; Dencausse, A.; Bacri, J.-C.; Luciani, N.; Gazeau, F. Nanomagnetic Sensing of Blood Plasma Protein Interactions with Iron Oxide Nanoparticles: Impact on Macrophage Uptake. *ACS Nano* **2012**, *6*, 2665–2678.
- (50) Lartigue, L.; Alloyeau, D.; Kolosnjaj-Tabi, J.; Javed, Y.; Guardia, P.; Riedinger, A.; Péchoux, C.; Pellegrino, T.; Wilhelm, C.; Gazeau, F. Biodegradation of Iron Oxide Nanocubes: High-Resolution *In Situ* Monitoring. *ACS Nano* **2013**, *7*, 3939–3952.
- (51) Dhakshinamoorthy, V.; Manickam, V.; Perumal, E. Neurobehavioural Toxicity of Iron Oxide Nanoparticles in Mice. *Neurotoxic. Res.* **2017**, *32*, 187–203.
- (52) Wu, J.; Zhu, Z.; Liu, W.; Zhang, Y.; Kang, Y.; Liu, J.; Hu, C.; Wang, R.; Zhang, M.; Chen, L.; Shao, L. How Nanoparticles Open the Paracellular Route of Biological Barriers: Mechanisms, Applications, and Prospects. *ACS Nano* **2022**, *16*, 15627–15652.
- (53) Donaldson, K.; Murphy, F. A.; Duffin, R.; Poland, C. A. Asbestos, Carbon Nanotubes and the Pleural Mesothelium: A Review of the Hypothesis Regarding the Role of Long Fibre Retention in the Parietal Pleura, Inflammation and Mesothelioma. *Part. Fibre Toxicol.* **2010**, *7*, 5.
- (54) Jones, J. S. P. The Pleura in Health and Disease. *Lung* **2001**, *179*, 397–413.
- (55) Hii, M.; Beyer, K.; Namin, S.; Malecki, K.; Schultz, A.; Rublee, C. Respiratory Diseases, Racial Disparities, and Residential Proximity to Coal Power Plants in Wisconsin, USA: A Cross-Sectional Study. *Lancet Glob. Health* **2021**, *9*, S19.